

REPORT DOCUMENTATION PAGE

Form Approved
OMB No. 0704-0188

Public reporting burden for this collection of information is estimated to average 1 hour per response, including the time for reviewing instructions, searching existing data sources, gathering and maintaining the data needed, and completing and reviewing this collection of information. Send comments regarding this burden estimate or any other aspect of this collection of information, including suggestions for reducing this burden to Department of Defense, Washington Headquarters Services, Directorate for Information Operations and Reports (0704-0188), 1215 Jefferson Davis Highway, Suite 1204, Arlington, VA 22202-4302. Respondents should be aware that notwithstanding any other provision of law, no person shall be subject to any penalty for failing to comply with a collection of information if it does not display a currently valid OMB control number. **PLEASE DO NOT RETURN YOUR FORM TO THE ABOVE ADDRESS.**

1. REPORT DATE (DD-MM-YYYY) 13-07-1998		2. REPORT TYPE Technical Paper		3. DATES COVERED (From - To)	
4. TITLE AND SUBTITLE Laser Induced Fluorescence Measurements on a Laboratory Hall Thruster (Postprint)				5a. CONTRACT NUMBER	
				5b. GRANT NUMBER	
				5c. PROGRAM ELEMENT NUMBER	
6. AUTHOR(S) W.A. Hargus, Jr. and M.A. Cappelli (Stanford Univ.)				5d. PROJECT NUMBER	
				5e. TASK NUMBER	
				5f. WORK UNIT NUMBER	
7. PERFORMING ORGANIZATION NAME(S) AND ADDRESS(ES) Air Force Research Laboratory (AFMC) AFRL/PRSS 1 Ara Road. Edwards AFB CA 93524-7013				8. PERFORMING ORGANIZATION REPORT NUMBER AIAA-1998-3645	
9. SPONSORING / MONITORING AGENCY NAME(S) AND ADDRESS(ES) Air Force Research Laboratory (AFMC) AFRL/PRSS 1 Ara Road Edwards AFB CA 93524-7013				10. SPONSOR/MONITOR'S ACRONYM(S)	
				11. SPONSOR/MONITOR'S NUMBER(S) AIAA-1998-3645	
12. DISTRIBUTION / AVAILABILITY STATEMENT Approved for public release; distribution unlimited.					
13. SUPPLEMENTARY NOTES Presented at the 34 th AIAA/ASME/SAE/ASEE Joint Propulsion Conference, Cleveland, OH, 13-15 July 1998. AIAA 1998-3645.					
14. ABSTRACT In this paper, we describe the results of a study of laser induced fluorescence velocimetry of neutral xenon in the plume of a Hall type thruster operating at powers ranging from 250 to 725 W. Neutral velocities are seen to increase with thruster discharge voltage. There is no evidence for neutrals being accelerated in the near field plume. Velocities appear to remain constant past the cathode plane. In preparation for future ion velocimetry studies, the plume plasma potential profile is measured for a number of conditions. For a low power condition, the plasma potential profile is mapped through the ionization region into the interior of the thruster. For this condition, the electric field profile is calculated. We also find evidence of neutral xenon streaming toward the Hall thruster. These backstreaming neutrals make determination of neutral xenon velocities difficult. We believe the neutrals originate from the thruster plume wall impingement approximately 2 m from the thruster.					
15. SUBJECT TERMS					
16. SECURITY CLASSIFICATION OF:			17. LIMITATION OF ABSTRACT	18. NUMBER OF PAGES	19a. NAME OF RESPONSIBLE PERSON
a. REPORT	b. ABSTRACT	c. THIS PAGE			19b. TELEPHONE NUMBER (include area code)
Unclassified	Unclassified	Unclassified	SAR	12	Dr. William A. Hargus, Jr. N/A

Laser Induced Fluorescence Measurements on a Laboratory Hall Thruster

W.A. Hargus, Jr.* and M.A. Cappelli**
Mechanical Engineering Department
Thermosciences Division
Stanford University
Stanford, CA 94305

Abstract

In this paper, we describe the results of a study of laser induced fluorescence velocimetry of neutral xenon in the plume of a Hall type thruster operating at powers ranging from 250 to 725 W. Neutral velocities are seen to increase with thruster discharge voltage. There is no evidence for neutrals being accelerated in the near field plume. Velocities appear to remain constant past the cathode plane. In preparation for future ion velocimetry studies, the plume plasma potential profile is measured for a number of conditions. For a low power condition, the plasma potential profile is mapped through the ionization region into the interior of the thruster. For this condition, the electric field profile is calculated. We also find evidence of neutral xenon streaming toward the Hall thruster. These backstreaming neutrals make determination of neutral xenon velocities difficult. We believe the neutrals originate from the thruster plume wall impingement approximately 2 m from the thruster.

Introduction

Due to their high specific impulse and high thrust efficiencies, Hall thrusters are now being considered for use on commercial, research, and military spacecraft. This technology provides economic advantages for a number of missions that can be translated into lower launch mass, longer time on station, or larger payloads [1].

There is a need for an increased understanding of the complex phenomena that govern the operation of Hall thrusters. In order to more fully understand the physics in these discharges, several laboratory model Hall thrusters have been constructed at Stanford University. These thrusters serve primarily as test articles for plasma diagnostics. These diagnostics include laser induced fluorescence (LIF), probes of various types, and thrust measurements [2-6].

Laser based techniques have been developed to nonintrusively probe neutral and ionized xenon [6]. Such measurements in the plumes of Hall and other types of ion thrusters provide information on the plasma discharge that is required to develop insight into the physical

processes occurring within the thrusters. Similar optical diagnostic measurements have been previously employed to examine plasma properties in other electric propulsion devices. For example, the hydrogen arcjet has been extensively studied using lasers to measure velocity, temperature, and electron number density [7]. The high spatial resolution of single-point laser-induced fluorescence is essential in probing nonuniform plasma environments such as those in Hall thrusters and other electric propulsion devices.

Theory

Laser Induced Fluorescence

The interaction of a laser beam with a plasma may involve the optical excitation of a number of atoms to a higher energy state. The excitation is more likely to occur if the laser is tuned to the energy difference, $h\nu_{12}$, between an upper state and lower state. The interaction can be investigated by either monitoring the resulting reduction in laser power following propagation through the plasma (absorption process), or by monitoring the subsequent spontaneous emission

* Student Member AIAA

** Member AIAA

as the resulting excited state relaxes to a lower state (laser-induced fluorescence process). Monitoring the fluorescence as the laser is tuned over the transition provides a measure of the fluorescence excitation line shape and is favored for the higher spatial resolution that it affords in the determination of plasma parameters. The spatial resolution for LIF is determined by the intersection of the probe laser beam with the optical collection volume at the probe volume.

If the absorber has a velocity component, u , along the axis of the laser beam, it will absorb the light at a frequency shifted from that of stationary absorbers because of the Doppler effect. The magnitude of this frequency shift depends on the velocity along the laser beam axis by

$$\delta\nu_{12} = \nu_{12} \frac{u}{c} \quad (1)$$

where c is the speed of light. The Doppler shift of a species' fluorescence profile away from the line center ν_{12} of stationary absorbers is in proportion to the species velocity.

The measured fluorescence signal is given by [8-10]

$$S_j = \eta_d \alpha_c h \nu_{12} A N_2 \quad (2)$$

where η_d is the efficiency of the detection system, α_c accounts for factors involving the collection system, and A is the Einstein coefficient for spontaneous emission of the relevant transition.

For low laser intensities, rate equation analysis indicates that the upper level population N_2 and therefore the fluorescence signal is linearly dependent on I_ν at steady state, i.e.,

$$N_2 \sim I_\nu B_{12} \phi_\nu \quad (3)$$

where I_ν is the spectral irradiance at frequency ν and B_{12} is the Einstein stimulated absorption coefficient, ϕ_ν is the transition's spectral line shape which accounts for the variation of the absorption or laser excitation with frequency. The line shape is determined by the environment of the absorbing atoms, so an accurate measurement of the line-shape function can lead to the determination of plasma parameters.

Several factors can affect the line shape and give rise to a broadening and/or shift of the spectral line. In high temperature plasmas, the most significant of these is due to the Doppler effect and gives rise to Doppler broadening. Doppler broadening reflects the fact that the absorbing species is distributed in velocity according to the kinetic temperature, T_{kin} . When the absorbing species is characterized by a Maxwellian velocity distribution, Doppler broadening results in a Gaussian line shape.

Collisional interactions between the absorbers and other species in the plasma give rise to spectral line shapes that are often Lorentzian. This includes interactions with charged particles (Stark broadening) and uncharged particles (van der Waals broadening). If both Doppler broadening and collision broadening are important and independent, the resulting line shape is a convolution of the Gaussian and Lorentzian line shape into a Voigt line shape.

The measured fluorescence excitation line shape is not necessarily equivalent to the spectral line shape. The line shape is an intrinsic property of the absorbers, whereas the fluorescence excitation line shape is the variation in the detected fluorescence signal with frequency as the laser is tuned across the absorption line feature. If the laser excitation significantly perturbs the populations in the coupled levels, it is said to be saturating the transition and the fluorescence signal is then a nonlinear function of laser intensity. In cases where the laser intensity is significantly below the saturation level and the laser linewidth is small compared to the measured linewidth, the fluorescence excitation line shape reflects the spectral absorption line shape as given by Eqns. 2 and 3. When the laser intensity is sufficiently high to saturate the transition, the fluorescence excitation line shape is broader than the spectral line shape and the fluorescence intensity is less than it would be if it were linear with the laser intensity I_ν . The saturation intensity, defined as that intensity which produces a fluorescence signal half of what it would be if the fluorescence was linear with I_ν , depends inversely on the line strength of the particular line. Stronger transitions have a smaller saturation intensity and thus a larger saturation effect for a given laser intensity.

Xenon Spectroscopy

The ground state of the xenon atom is not easily accessible to LIF. With available laser wavelengths it is advantageous to probe more accessible excited states. The spectroscopy of the $6s[3/2]_2^o - 6p[3/2]_2$ transition at 823.2 nm examined in this study is discussed elsewhere [11]. The conventional Racah notation for the inert gases is used to denote the levels investigated. Briefly, the seven isotopes each have a slight difference in their transition energies due to their differences in mass. The odd mass isotopes are further spin split due to nuclear magnetic dipole and nuclear electric quadrupole moments. The isotopic and nuclear-spin effects contributing to the hyperfine structure decomposes the $6s[3/2]_2^o - 6p[3/2]_2$ transition into 21 lines.

As is the case with neutral xenon, the ground state of the xenon ion is not easily accessible to LIF. The only ionic xenon transition for which the isotopic and hyperfine splitting constants are known is the 605.1 nm transition arising from the metastable $5d[3]_{7/2}$ ($^4D_{7/2}$) state. In this case, the combined isotopic and nuclear-spin effects cause the 605.1 nm transition to have 19 isotopic and hyperfine components contributing to its line shape. Previous work has utilized nonresonant fluorescence at 529.2 nm collected from the $6p[2]_{3/2}^o$ ($^4P_{3/2}$) upper state [6].

For LIF measurements aimed at only determining the velocity of the plasma flow, it is often convenient to probe more accessible transitions for which there is incomplete knowledge of the isotopic and nuclear spin splitting constants. Manzella has shown that the ionic xenon transition at 834.7 nm, $5d[4]_{7/2} - 6p[3]_{5/2}$, can be used to make velocity measurements in the plume of a Hall thruster [12-13]. In this case, the combined isotopic and nuclear-spin effects cause the 834.7 nm transition to have 20 isotopic and hyperfine components contributing to its line shape. An additional convenient feature of this transition is a strong line emanating from the same upper state. The $6s[2]_{1/2} - 6p[3]_{1/2}$ transition at 541.9 nm allows for nonresonant fluorescence collection.

Local electric and magnetic fields can also affect the spectroscopy of a transition. A magnetic field splits each fine or hyperfine line into a number of lines. An extremely strong electric field can also cause a splitting of spectral lines. Furthermore, perturbations of an atom's energy levels by nearby charged particles lead to a broadening and a shift of a spectral line. This Stark shift has a linear dependence on the electron number density, n_e , at the probe volume [14].

Plasma Potential Measurements

When an electrically isolated conductor is placed in contact with a plasma, the conductor will generally float at a potential different than that of the plasma potential [15]. This is due to the formation of a sheath. The more mobile electrons are depleted near the surface and an electron retarding sheath causes the conductor to float at a potential lower than the plasma potential.

One method to determine the plasma potential is to heat a probe until a sufficient number of electrons are thermionically emitted from the probe surface to neutralize the sheath. Once the sheath is neutralized, the probe will float at the local plasma potential. An advantage of using an emissive probe instead of a swept probe is the issue of cleanliness. Oxide layers on swept probes are difficult to remove and distort the current-voltage characteristic. When heated, emissive probes remove this oxide layer. They are thus cleaned in the course of their operation.

The relationship between the plasma potential and the floating potential can be determined for a collisionless plasma by examining the ion, Γ_i , and electron, Γ_e , fluxes.

$$\Gamma_i = n_s u_s \quad (4)$$

$$\Gamma_e = \frac{1}{4} n_s \bar{v}_e \exp\left(\frac{\phi_f - \phi_p}{T_e}\right) \quad (5)$$

where n_s is the plasma density at the sheath edge, u_s is the drift velocity of the ions at the sheath edge, ϕ_f is the surface floating potential, ϕ_p is the plasma potential, T_e is the electron temperature, and \bar{v}_e is the electron mean thermal speed given by

$$\bar{v}_e = \sqrt{\frac{8kT_e}{\pi m}} \quad (6)$$

where k is Boltzmann's constant and m is the electron mass. Several assumptions have been made in Eqns. 4 and 5. First, the ion flux is assumed to be constant. Second, the electron flux to the surface is retarded by a sheath. This sheath is assumed to affect only the electrons which have significantly lower masses than the ions.

An estimate for the sheath edge ion velocity is obtained from the Bohm criterion [15]:

$$u_s \geq u_B = \sqrt{\frac{kT_e}{M}} \quad (7)$$

where M is the ion mass and u_B is the Bohm drift velocity. Strictly, Eqn. 7 only applies to a collisionless, field free, stationary plasma. However, it does provide a lower bound estimate of the speed of the ions entering the sheath [16].

In the steady state case of a floating conductor in a plasma, the difference between the plasma and floating potentials can be determined by equating the fluxes of Eqns. 4 and 5, and substituting Eqns. 6 and 7 for the electron and ion speeds. This result is

$$\phi_f - \phi_p = -T_e \ln\left(\frac{M}{2\pi m}\right)^{1/2} \quad (8)$$

With Eqn. 8, the plasma potential difference can be calculated if the electron temperature is known. Conversely, if the plasma and floating potentials are known, an acceptable approximation to the electron temperature may be determined. Finally, if the plasma potential field is sufficiently well known, it can be numerically differentiated to yield the electric field, \bar{E} .

$$\bar{E} = -\nabla\phi_p \quad (9)$$

Test Apparatus

Test Facility

The Stanford high vacuum test facility consists of a non-magnetic stainless steel vessel approximately 1 m in diameter and 1.5 m in length. The facility is pumped by two 50 cm diffusion pumps backed by a 425 l/s mechanical pump. Base pressure of the facility with no flow is approximately 10^{-6} Torr as measured by an ionization gauge uncorrected for gas species. Chamber pressures during thruster testing at

xenon flow rates of approximately 2.3 mg/s result in chamber background pressures of in the region of 10^{-4} Torr. This indicates that the facility has a xenon gas pumping speed of approximately 2,000 l/s. Propellant flow to the thruster anode and cathode is controlled by two Unit Instruments 1200 series mass flow controllers factory calibrated for xenon. The propellant used in this study was research grade (99.995%) xenon.

Hall Thruster

The thruster used in this study has 4 outer magnetic windings consisting of 89 mm long, 25 mm diameter, cores of commercially pure iron wrapped with 6 layers of 22 gauge insulated copper magnet wire. The inner core is also 25 mm in diameter and 89 mm in height and has 12 layers of magnet wire. A cutaway view of the thruster is shown in Fig 1. The depth of the electrical insulator is 84 mm. The insulator is constructed from 2 sections of cast 99.9% alumina tubing cut to length. These two pieces are cemented to a machinable alumina plate attached to the back plate of the thruster with non-conducting fasteners (not shown). This thruster is modification of the thruster presented in Ref. 5. The primary modification is to the outer magnetic cores which were increased in diameter to 25 mm from 9.5 mm. This modification increased the radial magnetic field strength of the thruster significantly, but has not affected the profile of the magnetic field, or its peak location. More detailed information on the magnetic field characteristics can be found in Ref. 5. One additional modification is a boron nitride layer on the front surface of the thruster. This layer does not appear to affect the operating characteristics of the thruster. However, the boron nitride layer prevents iron from the thruster body from sputtering and redepositing on to the insulating channel.

The insulator supports the 90 mm outer diameter stainless steel anode. Propellant distribution through the anode is accomplished by 32 evenly distributed holes each with a diameter of 0.5 mm. The anode is secured from below the insulator by three alumina bolts (not shown) which secure the anode and the insulator to the thruster body. An isolated stainless steel feed provides electrical and propellant feeds to the discharge.

Laser Induced Fluorescence

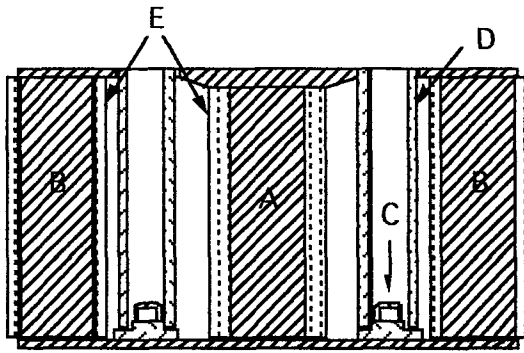


Fig. 1. Cross-section of modified Hall thruster. (A) central magnetic core, (B) outer magnetic cores, (C) anode, (D) insulated acceleration channel, and (E) magnetic windings.

The cathode required to neutralize the ion beam and support the necessary electric field is an Ion Tech, Inc. HCN-252 hollow cathode. It is capable of supporting a maximum emission current of 5A. It is mounted to the rear of the thruster on a stainless steel bracket such that the plane of the cathode exit is 20 mm beyond the thruster exit plane.

The anode discharge is powered by a Sorenson DCR300-6 laboratory power supply capable of providing 300 V and 6 A. The cathode heating element is powered by a Powerstat variable transformer supplying 8.5 A required to initially heat the cathode for startup and 4.0 A during thruster operation. The cathode keeper uses a Sorenson SCR600-1.7 high voltage power supply which provides 250 V in initiate cathode startup and approximately 10 V and 250 mA during thruster operation. Both the anode and cathode keeper power lines are connected to the discharges through 4 Ω power resistors which act as electrical ballasts during the discharge start. The power required for the magnetic circuit solenoids is provided by a current controlled power supply producing 100-500 mA of DC current.

The thruster is mounted on a two axis translation system. In the vertical, the thruster has a range of travel of approximately 30 cm. In the axial, or horizontal, direction, the thruster is constrained to a total travel of approximately 6 cm. Both stages have resolutions on the order of 10 μm , although the repeatability is considerably courser.

The experimental apparatus used for the laser induced fluorescence measurements consists of a tunable Coherent 899-21 single frequency titanium sapphire laser. The laser is actively stabilized to provide line widths on the order of 1 MHz with near zero frequency drift. Scan widths of up to 20 GHz can be realized at center wavelengths between 680 to 1060 nm. The titanium sapphire laser is pumped by Coherent solid state Verdi pump laser. The pump laser provides 5 W of single mode pump power at 532 nm. The laser wavelength was monitored by a Burleigh Instruments WA-1000 scanning Michelson interferometer wavemeter with a resolution of 0.01 cm^{-1} .

Figure 2 shows the experimental apparatus for the LIF velocimetry measurements. The probe beam is directed into the Hall thruster plume by a series of mirrors. The slightly divergent beam (1.7 milliradians full angle) is focused to a submillimeter beam waist at the thruster exit by a 50 mm diameter, 1.5 m focal length lens.

The collection optic consists of a 75 mm diameter, 60 cm focal length, collimating lens. The collected light is then focused on to the entrance slit of a 0.5 m Ebert-Fastie monochromator with a 50 mm diameter, 30 cm focal length, lens. An optical field stop is placed between the two lenses to match the $F/\#$ of the optical train with that of the monochromator.

The monochromator is used as a narrow band optical filter so that only light from the transition of interest is collected. With entrance and exit slits full open (425 μm), the 600 groove/mm plane grating blazed for 600 nm within the monochromator allows the Hamamatsu R928 photomultiplier tube (PMT) to sample a wavelength interval of approximately 1 nm. The orientation of the monochromator allows the height of the slits to define the length of the probe beam along which the fluorescence is collected. Prior to each test and with the PMT housing removed, a HeNe laser is reversed through the entire collection optical train to insure the alignment with the probe beam.

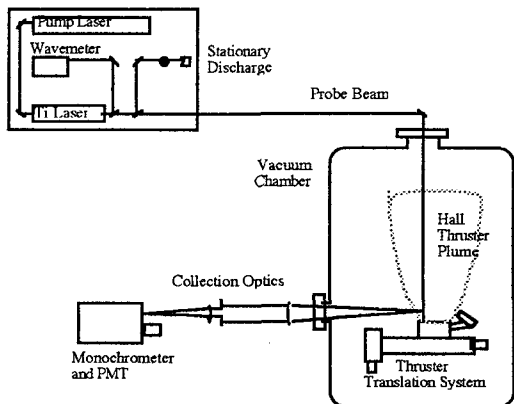


Fig. 2. LIF velocimetry apparatus with laser system and collection optics.

A portion of the probe beam is split from the main beam and passed through a xenon glow discharge tube, used as an stationary absorption reference. A silicon photodiode monitors this signal. The use of a glow discharge tube for this purpose is only possible for neutral xenon. The glow discharge does not support a sufficient population of excited state ions for detection.

The LIF signal is collected using a Stanford Research Systems SRS-850 digital lockin amplifier. The probe beam is chopped by a SRS-540 optical chopper. The absorption signal from the stationary reference is collected using a SRS-530 lockin amplifier. Data from the absorption signal, laser power output, and the wavemeter are stored on the SRS-850 using 3 available analog inputs along with the LIF signal.

Typical tests consist of a 0.4 cm^{-1} scan of the probe laser frequency over a 10 minute period. The beam is chopped at a frequency of 1.5 kHz. Both lockin amplifiers use 3 s time constants. Data is sampled at 2 Hz, producing four traces of approximately 1,200 points for each velocity data point.

Plasma Potential Probe

The plasma potential probe is constructed from $150 \mu\text{m}$ diameter 2% thoriated tungsten wire. The filament is formed by winding the thoriated wire around a 0.9 mm mandrel for 8 turns for a total length of approximately 1 cm. The filament is suspended between two 0.50 mm diameter tantalum wires with an approximate separation of 5 mm. The tantalum wires are sheathed in 1.25 mm diameter alumina tubes. The probe is similar to those used in previous

Hall thruster studies [17]. Figure 3 shows a schematic of the probe electrical circuit.

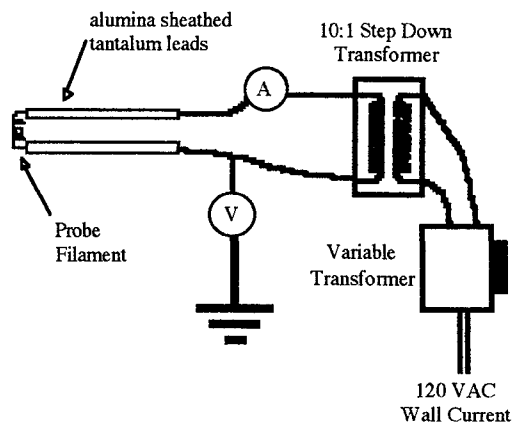


Fig. 3. Plasma potential probe circuit schematic.

The probe is heated using a 10:1 step down transformer powered by a 10 A Powerstat manual variable transformer (Variac) which is connected to wall current (120 V, 60 Hz). This transfers AC power to the probe while allowing the probe circuit to float at the plasma potential.

The probe filament is placed inside the vacuum chamber on a translation stage with a 15 cm range of motion along the thruster's axial direction. This allows the thruster to move in the vertical direction and the probe to move axially into and out of the thruster plume. The isolating transformer and the variable transformer are located outside the chamber. The voltage of the floating portion of the probe is monitored relative to ground by a hand held DC digital voltmeter ($>100 \text{ k}\Omega$ impedance). The probe current is monitored with a hand held AC ammeter to ensure repeatable results.

The test procedure consists of placing the probe in the required location. The floating potential is recorded, the probe current is raised to 4 A, and then the heated probe potential is recorded. The procedure is then repeated.

Results and Analysis

Operating Conditions

The Hall thruster was operated at four conditions. At each of these conditions, the peak magnetic field was measured to be approximately 175 G, the mass flow to the anode was 2 mg/s, mass flow to the cathode was 0.3 mg/s. The four conditions corresponded to discharge voltages of 100, 160, 200, and 250 V. The

anode currents for these conditions were 2.1, 2.4, 2.6, and 2.9 A, respectively. The total power consumed by the cathode and magnet circuit was approximately 30 W. It should be noted that the power dissipated in the ballast resistors on the anode and cathode keeper lines (~10 W) are not included in these calculations.

Neutral Xenon Velocimetry

Figure 4 shows exit plane velocities measured at the center of the discharge channel for a number of anode voltages. The sample volume for all neutral data presented in this work is approximately $100\mu\text{m}$ in diameter and 6 mm in length. This length was required for adequate signal strength. Background emission was approximately a factor of 300 greater than the LIF signal. As seen in Fig. 4, the neutral exit velocities increase with discharge voltage. This behavior is likely due to two phenomena. First, as the discharge power increases, the anode should rise in temperature. If the neutral flow is independent of the ionic flow, the neutrals would at best reach sonic velocities which would increase with the square root of the anode temperature. On the other hand, if the ions are colliding with the neutrals in sufficient numbers, the neutrals may be accelerated by collisions with the ions. If so, the velocity of the neutrals will depend on the velocity of the ions which varies with the square root of the discharge voltage. With thruster power primarily a function of the discharge voltage, the ability to distinguish between these two processes is impossible without temperature measurements of the anode.

Shown in Fig. 5 is a portion of a exit plane radial profile for a discharge voltage of 160 V. The profile is relatively constant up the edge of the discharge channel at 6 mm. When the volume 3 mm beyond the edge of the acceleration channel is examined. It reveals an interesting result. The correlation between the stationary discharge implies that the velocity is approximately 0 m/s. A closer examination of the LIF trace reveals that the peak may consist of two almost superimposed peaks. This would indicate that two distinct velocity classes of neutrals exist. The fit of two such signal to the data implies that the two velocities on the order 230 and -150 m/s. These are indicated on Fig. 5 by the round symbols.

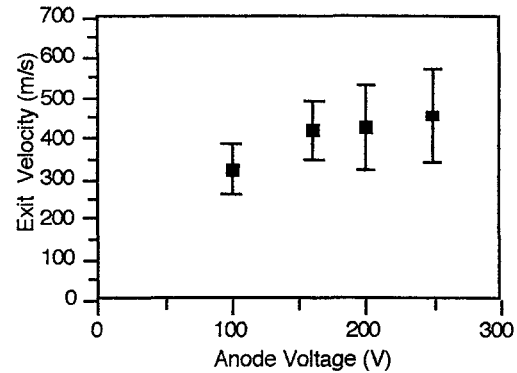


Fig. 4. Channel centerline velocities at a number of discharge voltages.

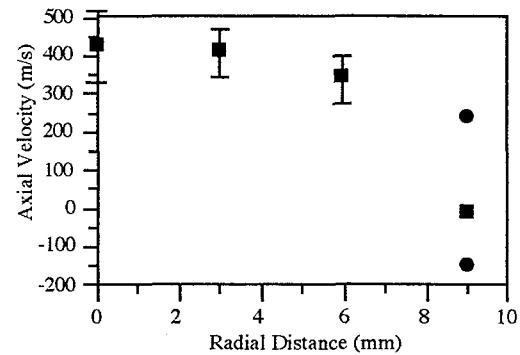


Fig. 5. Radial Variation of axial velocity at a discharge voltage of 160 V.

This phenomena was also seen downstream in velocity measurements in the plume. Figure 6 shows the evolution of the line shape in to the plume at a discharge voltage of 200 V. Figure 6D shows a more extreme case of bimodal velocities at a discharge voltage of 250 V. The dashed lines in these figures represent the absorption line shape of the stationary reference.

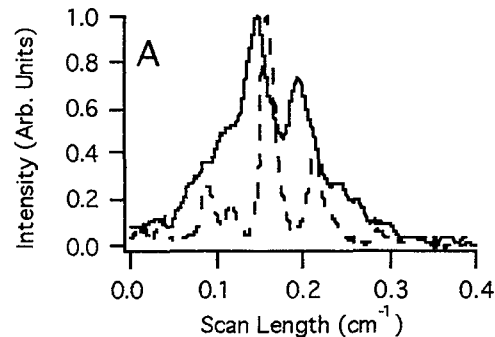


Fig. 6A. Progression of LIF line shift evolution with distance from exit plane: positive velocity at 3 mm. Voltage discharge of 200 V.

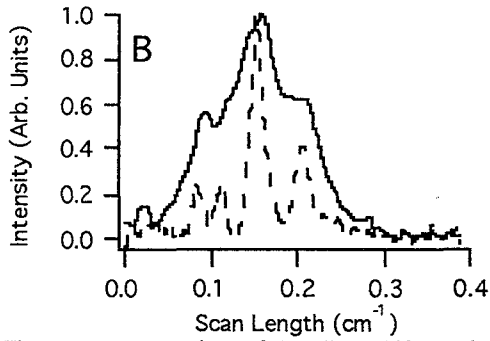


Fig. 6B. Progression of LIF line shift evolution with distance from exit plane: possible bimodal velocity behavior at 7.5 mm. Voltage discharge of 200 V.

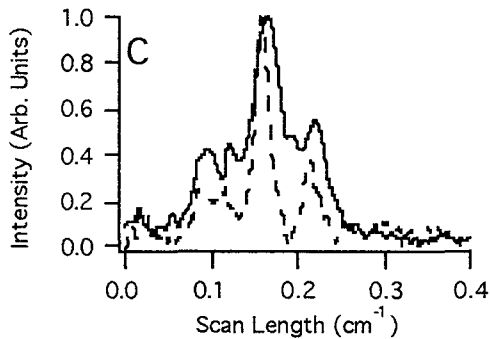


Fig. 6C. Progression of LIF line shift evolution with distance from exit plane: negative velocity at 15 mm. Voltage discharge of 200 V.

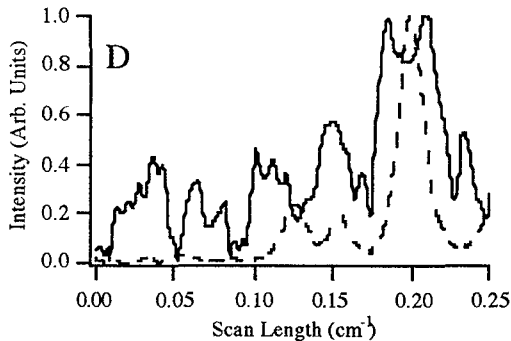


Fig. 6D. Extreme case of bimodal behavior seen near the exit plane for a discharge voltage of 250V.

Once this unexpected shift was found in the plume, one possible source could be dismissed. Near the thruster exit, the magnetic and electric fields would be the strongest. If either Zeeman, or Stark splitting of degenerate lines were to occur, it would occur near the thruster. The point in Fig. 5 at 9 mm from the channel center is near to the inner magnetic core and the initial concern was that Zeeman splitting was appearing. With this same behavior, now

occurring away from the thruster, the conclusion reached is that there are two relatively distinct populations of neutrals with diametrically opposed velocities.

Before proceeding further, the LIF line shapes in Fig. 6 need some explanation. The excitation line shapes are distinctly more broad than the absorption line shapes. This is due to partial saturation of the transition by the laser probe beam. The laser system was capable of producing 200 mW at this wavelength. For the data presented, neutral density filters were used to attenuate the laser output. The power delivered to the probe volume was generally on the order of 2 mW. Laser powers less than this did not produce a recognizable signal that could be correlated with the stationary reference absorption line shape to determine a velocity.

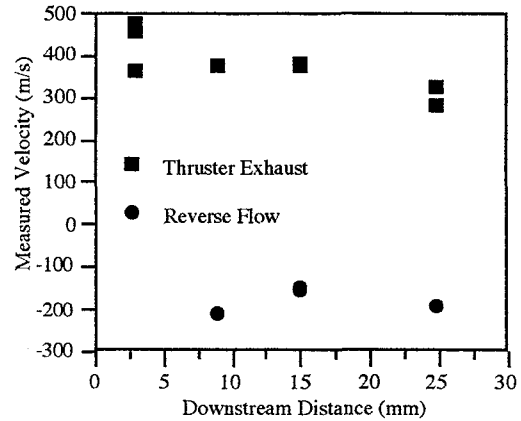


Fig. 7. Axial near field plume velocities at a discharge voltage of 250 V.

The highest discharge voltage, 250 V, produced the highest neutral velocities. The population of the reversed flow was also larger as evidenced by the bimodal peak visible near the exit plane in Fig. 6D. The larger magnitude of both velocities shifted the two superimposed excitation line shapes further apart. Estimates of the thruster exhausted neutral velocities in the plume are shown in Fig. 7 for a discharge voltage of 250V. The data were calculated by subtraction of the reversed flow contribution to the LIF excitation line shape. This contribution was modeled by use of an unsaturated line shape. There is much uncertainty in this procedure. No corrections were made for the partial saturation of the excitation line shape. The velocities calculated in this manner are presented along with a number of points near the exit plane which exhibited little evidence of the reverse velocity neutrals. Also included in Fig. 7 are several of the calculated reverse velocities at this condition.

These appear to have a nearly constant velocity of approximately -200 m/s. Although error bars are not shown in Fig. 7, the uncertainties in the velocities are on the order to 25% near the exit plane and increase further in the plume as the reversed velocity neutrals begin to dominate the LIF signal.

The source of the reversed velocity neutrals is of considerable importance, that it may be eliminated. During the later portion of the tests performed for this paper, it was discovered that the plume of the thruster was extending into a portion of the vacuum chamber over a diffusion pump. During this time, the laser window used in this study was coated with decomposed diffusion pump oil. In addition, the pumping speed of the vacuum system was degraded. A conical stainless steel baffle was placed before the diffusion pump to deflect the ion beam away from the window. Later analysis of LIF data taken with the baffle in place indicates that the baffle increased the amount of back flow significantly. It is important to note that the back flow was evident before the placement of the baffle, although to a lesser extent. It is therefore, almost certain that the xenon neutral back flow is due to reflected plume flow off the wall, and the baffle.

Plasma Potential Measurements

Plasma potential measurements were performed for two reasons. First, to explore the structure of the electric field near the thruster to determine whether the features seen in the LIF velocimetry data were in fact due to Stark effects. The second and most important reason was to determine the plasma potentials of the thruster near plume flow field in preparation for ion velocity measurements. Since the Hall thruster is an electrostatic accelerator, knowledge of the plasma potential is important to understanding where the propellant acceleration occurs. The correspondence between the ion velocity measurements and the plasma potential measurements will provide an indication of the efficiency of the propellant acceleration process.

Figure 8 shows the plasma potential measurements. The measurements were made in the center of the acceleration channel and extend from approximately 50 mm into the plume, to the thruster exit plane. Just inside the exit plane, the probe experienced severe heating. One of the alumina sheaths would usually become incandescent. At this point, the unheated probe potential would rise to near the plasma potential

as the probe was heated by the plasma. The probe was removed promptly from within the thruster when this occurred. Examination of the probe after these incidents, revealed that the alumina had become semi-molten. For the 100 V discharge voltage case, the probes did not heat and measurements were taken until the plasma potential leveled.

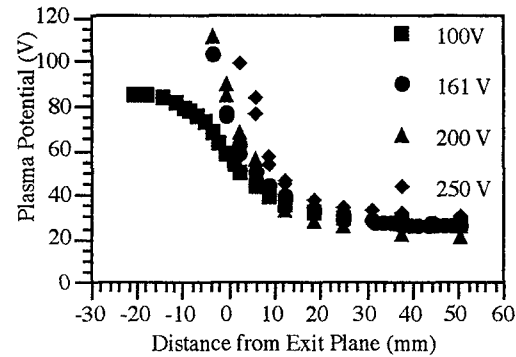


Fig. 8. Plume plasma potential data at discharge channel center.

The plasma potential is nearly constant in the plume and rises significantly near the exit plane. For the 100 V anode potential case, it is possible to numerically differential the plasma potential data to produce the profile of the electric field shown in Fig. 9. The electric field peaks at the same location as the magnetic field, although the electric field profile is narrower [5]. Examining Fig. 8, the plasma potential for this case appears to level out near 85 V, 15 V below the anode potential. This is consistent with the Von Engle theory which predicts that the anode fall of a glow discharge is somewhat greater than ionization potential of the gas in question (Xenon ~12.2 eV) [18].

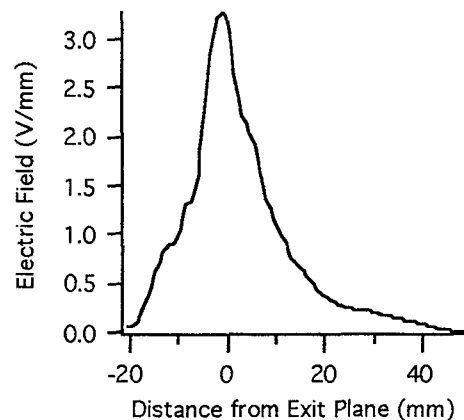


Fig. 9. Electric field as calculated from plasma potential measurements for a discharge voltage of 100V.

Using floating and plasma potentials, an estimate of the electron temperature can be calculated by using Eqn. 8 as shown in Fig. 10. The electron temperatures quickly rise with the plasma potential. With only the exception of the 100 V case, the electron temperatures rise above the xenon ionization potential near the exit plane, implying that ionization may be occurring in this region.

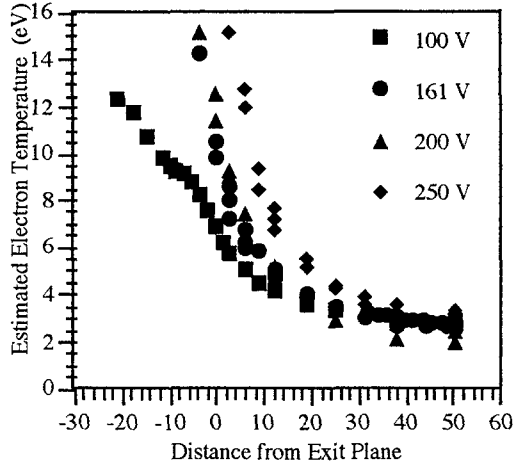


Fig. 10. Electron temperatures calculated from floating and plasma potentials using Eqn. 8.

For the 250 V discharge voltage case, a radial profile of the plasma potential across the acceleration channel and approximately 13 mm downstream of the exit plane is shown in Fig. 11. The electron temperature follows the plasma potential closely. Similar structure has been seen further into the plume as well.

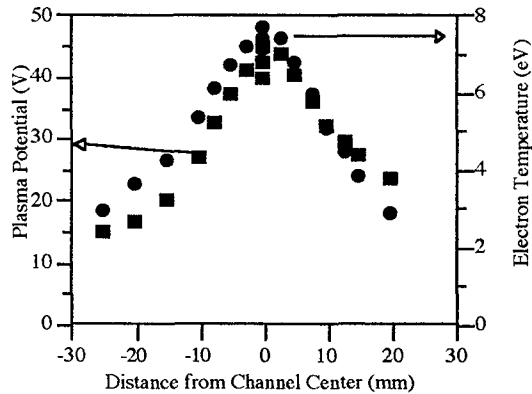


Fig. 11. Cross-section of plasma potential and electron temperature across the acceleration channel at a distance of 13 mm from the exit plane at a discharge voltage of 250 V. Note that the acceleration channel is 12 mm wide.

The plasma potential data confirms that while large electric fields do exist in the Hall thruster, they do not reside in the plume and as such are not responsible for the distorted LIF excitation line shapes. The plasma potential data has given an indication of the energies of the xenon ions. Therefore, the ionic velocities can be approximated and used as a starting point for LIF velocimetry.

Ionic Xenon Velocimetry

Measurements of ionic xenon velocities have not been completed. The 824.7 nm transition is accessible with the same laser and optical system as the neutral 823.2 nm line. At this time, only a small amount of work has been completed. For example, Fig. 12 shows a LIF excitation signal of the 834.7 nm transition. These data was taken at a discharge voltage of 85 V. The line shape is shifted approximately 0.29 cm^{-1} , corresponding to a velocity of approximately 7.2 km/s. This transition is useful because of its accessibility, but in order to determine the ionic temperature, the ionic transition at 605.1 nm, where the isotopic and hyperfine splitting constants are known, must be used.

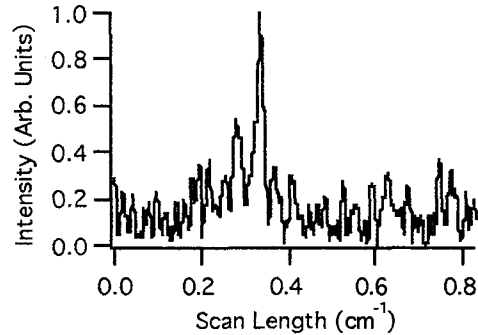


Fig. 12. LIF trace of ionic xenon transition at 834.7 nm.

Conclusions and Future Work

From the data available, the neutral velocity does not appear to increase in the near field plume. The neutrals appear to exit at velocities between 300 and 600 m/s. The velocities appear to remain relatively constant, at least until the cathode plane at 20 mm. Reliable neutral velocity measurements any further into the plume are not possible at this time. The magnitude of the neutral velocity corresponds to previous work, but it is now believed that the deceleration of the neutrals evident in those

measurements was caused unaccounted by reverse flowing neutrals [6].

The backstreaming neutrals are believed to be a specular reflection of the recombined thruster ion beam. It should be possible to minimize this effect by changing the orientation of the surfaces upon which the plume impinges. This should allow the unambiguous determination of neutral velocities in the plume. The question of what effect this back flow has on the thruster operation must also be answered before further measurements can be performed.

The plasma potential measurements were successful in measuring the plasma potential curves in the near plume. However, the inability of the probe to enter the thruster at higher discharge voltages is an issue will be pursued. Future efforts will include a more robust probe able to survive entrance into the acceleration channel at these conditions.

A possible solution to some of the facility issues will be the new high vacuum facility constructed for our laboratory. It consists of a stainless steel vacuum vessel, 1.3 m in diameter, and 3 m in length. It is pumped by two 1.2 m cryo-pumps with a combined rated speed on xenon of 67, 000 l/s at 5×10^{-6} Torr. This facility is expected to be fully functional by October 1998.

Acknowledgments

This work is supported by the Air Force Office of Scientific Research. W.A. Hargus, Jr. is supported under the Air Force Palace Knight Program.

References

1. F.S. Gulczinski and R.A. Spores, "Analysis of Hall-Effect Thrusters and Ion Engines for Orbit Transfer Missions," AIAA-96-2973, 32nd Joint Propulsion Conference, July 1-3, 1996, Lake Buena Vista, FL.
2. R.J. Cedolin, W.A. Hargus, Jr., R.K. Hanson, and M.A. Cappelli, "Laser Induced Fluorescence Diagnostics for Xenon Hall Thrusters," AIAA-96-2986, 32nd Joint Propulsion Conference, July 1-3, 1996, Lake Buena Vista, FL.
3. R.J. Cedolin, W.A. Hargus, Jr., R.K. Hanson, and M.A. Cappelli, "Laser Induced Study of a Xenon Hall Thruster," AIAA-97-3053, 33rd Joint Propulsion Conference July 6-9, 1997, Seattle, WA.
4. W.A. Hargus, Jr., N.B. Meezan, and M.A. Cappelli, "Transient Behavior of a Low Power Hall Thruster," AIAA-97-3050, 33rd Joint Propulsion Conference July 6-9, 1997, Seattle, WA.
5. W.A. Hargus, Jr., R.J. Cedolin, N.B. Meezan and M.A. Cappelli, "A Performance Study of a Low Power Hall Thruster," AIAA 97-3081, 33rd Joint Propulsion Conference July 6-9, 1997, Seattle, WA.
6. R.J. Cedolin, W.A. Hargus, Jr., P.V. Storm, R.K. Hanson, and M.A. Cappelli, "Laser-induced Fluorescence Study of a Xenon Hall Thruster," *Applied Physics B: Lasers and Optics*, Vol. 65, pp 459-469, 1997.
7. P.V. Storm, *Optical Investigations of Plasma Properties in the Interior of a Arcjet Thrusters*, Thermosciences Division Report No. TSD-102, Ph.D. Dissertaion, Stanford University, 1997.
8. R. P. Lucht, "Applications of Laser-Induced Fluorescence Spectroscopy," in *Laser Spectroscopy and its Applications*, edited by L. J. Radziemski, R. W. Solarz, and J. A. Paisner, Marcel Dekker, New York, .
9. A.C. Eckbreth, *Laser Diagnostics for Combustion Temperature and Species*, Overseas Publishers Association, Amsterdam, 1996.
10. W. Demtroder, *Laser Spectroscopy: Basic Concepts and Instrumentation*, Springer-Verlag, Berlin, 1996.
11. R. J. Cedolin, R. K. Hanson, and M. A. Cappelli, "Semiconductor Laser Diagnostics for Xenon Plasmas," AIAA-94-2739, 30th Joint Propulsion Conference, June 27-29, 1994, Indianapolis, IN.
12. D.H. Manzella, "Stationary Plasma Thruster Ion Velocity Distribution," AIAA-94-3141, 30th Joint Propulsion Conference, June 27-29, 1994, Indianapolis, IN.
13. J. E. Hansen and W. Persson, "Revised Analysis of Singly Ionized Xenon, Xe II," *Physica Scripta*, Vol. 36, pp 602-643, 1987.
14. H. R. Griem, *Spectral Line Broadening by Plasmas*, Academic Press, New York, 1974.
15. M.A. Lieberman and A.J. Lichtenberg, *Principles of Plasma Discharges and Materials Processing*, John Wiley and Sons, Inc., New York, 1994.
16. F.F. Chen, *Introduction to Plasma Physics and Controlled Fusion: Volume 1*, Plenum Press, New York, 1990.
17. A.I. Morizov, Y.V. Esipchuk, G.N. Tilinin., A.V. Trofimov, Yu. A. Sharov, and G. Ya. Shshepkin, "Plasma Accelerator with Closed Electron Drift and Extended Acceleration Zone," *Soviet Physics - Technical Physics*, Vol. 17, No. 1, July 1972.
18. S.C. Brown, *Basic data of Plasma Physics: The Fundamental Data on Electrical Discharges in Gases*, American Institute of Physics, 1994.